AIAA 97-2492

CO_2 Vibrational Relaxation Effects in a Laser-Heated Hypersonic Flow

C. C. Limbaugh and J. A. Drakes
Sverdrup Technology, Inc., AEDC Group
Arnold Engineering Development Center
Arnold Air Force Base, Tennessee 37389

32nd Thermophysics Conference
June 23 - 25, 1997 / Atlanta, GA

CO_2 VIBRATIONAL RELAXATION EFFECTS IN A LASER-HEATED HYPERSONIC FLOW*

*C. C. Limbaugh** and J. A. Drakes†*
Sverdrup Technology, Inc., AEDC Group
Arnold Engineering Development Center
Arnold Air Force Base, TN 37389

Abstract

The establishment of flow conditions characteristic of hypersonic flight in a ground test facility by conventional means requires plenum conditions that have very high temperatures and give rise to a variety of materials problems. A well-known approach to solving these problems is to use high-pressure, moderate temperature plenum conditions and add energy as the flow expands through a carefully designed nozzle. A modern approach (Radiatively Heated Wind Tunnel) uses an HF laser to excite the $(02^{l}1)$ mode of CO_2 naturally present or added to the flow. One of the early challenges in the development will be to demonstrate the ability to add energy into the supersonic flow in a predictable and controllable manner. Consequently, a subscale experiment, the Laser Demonstration Device (LDD), is planned to investigate the transfer of laser energy to a small, expanding nozzle flow.

Previous modeling of the energy transfer of the laser energy into the gas for the LDD depended on a conventional two-temperature approach to describe the internal structure of the molecules and to determine the rate coefficients. Realizing that the detailed physics of the energy transfer was important to the description of the wind tunnel performance and, hence, its viability, an effort was undertaken to compute the effect of CO_2 relaxation using a technique in which the individual vibrational states are considered. Results of these computations are reported here.

The state-to-state approach has been utilized before in rocket exhaust flows where the densities are low and temperatures modest. Individual states of CO_2, N_2, and O_2 were maintained as distinct states, and relaxation rates for each state were determined. A vibrational temperature is not required. The laser excitation along the flow direction was described by an empirical absorption function and is the same as used previously. Feedback coupling between the laser absorption function and the state distributions is not included at the present level of approximation.

The results shown here are in agreement with earlier work; significant energy coupling to the flow and laser heating of the flow appears to be a feasible approach. However, the details of the vibrational relaxation show that a conventional two-temperature approach does not describe the resultant distribution. Consequently, inclusion of these effects will be required for successful prediction of exit plane properties, and thus, will be of critical importance to facility design and control.

Introduction

The development of hypersonic flight vehicles is seriously limited by the lack of ground test facilities that can routinely produce flows in excess of Mach 8. At these higher flight Mach numbers, reservoir conditions in conventional expansion-type wind tunnels become extreme enough that containment of the reservoir becomes a limiting factor on the tunnel operation. For example, to achieve a simulated flight condition of Mach 10 at 30-km simulated altitude (0.03 atm, 200 K), a simple calculation shows that chamber pressure in excess of 1,000 atm and temperatures in excess of 4,000 K are required. This temperature is well above the melting temperature of materials that can be used for wind tunnel construction. Additionally, at these

* The research reported herein was performed by the Arnold Engineering Development Center (AEDC), Air Force Materiel Command. Work and analysis for this research were performed by personnel of Sverdrup Technology, Inc., AEDC Group, technical services contractor for AEDC. Further reproduction is authorized to satisfy needs of the U. S. Government.

** Associate Fellow, AIAA.

† Senior Member, AIAA

high temperatures there is significant air chemistry, and the working gas delivered to the test article is not representative of the air at actual flight conditions. Further, at the high pressures, throat erosion can significantly degrade flow quality, even at lower temperatures. One approach to achieving these high Mach number flows has been to use facilities that operate for very short times so that materials degradation is minimal and accept whatever chemical effects are present. This approach limits test time for component testing and the chemistry effects seriously limit the utility for combustor development and testing.

An approach to attack this problem has been proposed[1] in which the energy is added with a high-power laser to the supersonic flow downstream of the throat. With this approach, the plenum can be at very high pressure but at a relatively cool temperature through the throat expansion, thus avoiding materials and air chemistry problems that characterize conventional approaches. This energy addition is accomplished through a portion of the flow in which the expansion is relatively slow (although maintained at supersonic speeds) and then a final expansion is accomplished to the desired Mach number and test conditions. Although there are other candidate methods for energy addition (e.g., electron beam, microwave, and magnetohydrodynamics), the use of high-power lasers has progressed farthest in the design studies and is the subject of this paper.

As described in Refs. 1-4, development of such a facility, the radiatively heated wind tunnel (RDHWT), presents several significant engineering challenges. Consequently, incremental proof-of-concept demonstrations are planned as part of the path toward development of a full-scale device. An early challenge that is critical to validating the feasibility of the approach is the demonstration of energy addition to a supersonic flow for an increase in the test chamber temperature and pressure under controllable and predictable conditions. Such a demonstration is quite feasible with HF or DF lasers that currently exist, and plans are proceeding to accomplish just such a demonstration. One approach for the demonstration is to use a 10-kW HF laser, the Laser Demonstration Device (LDD), with CO_2-seeded air flow. The high-power HF laser already exists, and it has been shown earlier[3] that there are several CO_2 absorption lines that are close to the laser lines. In the high-pressure environment planned for the absorption region, there will be significant coupling of the input laser energy into the CO_2. Subsequent transfer of the energy from the CO_2 into the kinetic modes of the flow was shown to be plausible based on a straightforward two-temperature relaxation model in which the N_2 - O_2 V-V transfer is the limiting rate for the relaxation. Although the feasibility model[3] indicated that there is significant coupling of the laser energy into the flow, in actuality the laser couples to specific vibrational states in the CO_2 and the details of the subsequent relaxation are not modeled in the conventional approach. Consequently, it was decided to investigate the thermalization of the input energy of the LDD experiment using a state-specific relaxation (SSR) model that includes the individual molecular vibrational states.[5-6]

The SSR model has the capability to model the individual molecular vibrational states participating in the laser absorption and subsequent thermalization as separate entities. Thus, each vibrational state considered becomes a separate species, its concentration is a result of the kinetic processes to which the molecules are subjected, and a state specific NLTE distribution is calculated. Vibrational temperature is not used explicitly, but rather may be a consequence if the excited states exhibit the properties characteristic of such a temperature, i.e., a Boltzmann distribution. The SSR model has been used previously to investigate the details of the CO_2 radiative transfer from rocket exhausts and includes the vibrational states participating in the present laser absorption and subsequent thermalization. An earlier study[6] showed that different distribution models can result in different radiative transfer properties, and it was surmised that including the details of the relaxation processes would show some differences in the predicted energy transfer to the medium.

In the present paper, the elements of the various models for modeling the laser addition to the flow are described. These elements include the specification of the LDD nozzle and power addition profile, the flow solver, the molecular model, the rate coefficients, and the thermodynamics. Results

of application to the LDD are described and the effect of the energy addition on the exit plane gas dynamic properties are examined. The internal state distributions are examined for their relevance to a conventional two-temperature approach and the effectiveness of the thermalization. Implications for the larger scale devices are drawn.

Models

Laser Demonstration Device Model

The nozzle contour used for the present study is shown in Fig. 1 and is similar to a contour proposed early in the effort. Although the exact contour of the nozzle is still in the design and development phase, the larger issues of examining the thermalization of laser energy can be studied without the exact contour. Common elements of all nozzle designs for subscale feasibility demonstration include the rapid expansion from the very small throat (0.28-cm diam here) to an area ratio of about 2, followed by a long region of constant or slowly increasing area ratio and then fairly rapid expansion to a larger area ratio (here about 90, exit diameter of about 2.6 cm). The reservoir conditions used for this demonstrator are 80 atm and 1,150 K. The working gas is air seeded with CO_2 to bring the mixture to 40-percent CO_2 and 60-percent air.

It is recognized that this model for an LDD nozzle with an area ratio of 90 gives an expansion to a Mach number of only 6 with no energy addition, which is far from what is required for a hypersonic facility. However, the near-term objectives are for the demonstration of energy addition into a supersonic stream in a predictable and controllable manner. Use of these more modest conditions fits well within the present experience base and will be relatively straightforward to accomplish. In this fashion, feasibility of the concept can be examined without requiring significant advances in the state of the art, and the ability to predict the exit plane conditions can be tested as well as developing the techniques for controlling the test chamber conditions.

The energy in the LDD is supplied with a 10-kW HF chemical laser and, except for power level, is expected to be similar to that described for larger devices.[3] The energy addition profile derived in the same manner as in Ref. 3 is shown in Fig. 2. It should be noted that this is a specified profile and is an input condition for the calculations reported here. Coupling between the present detailed model and the input laser beam has not been accomplished yet. As pointed out above, there are several laser lines nearly coincident with absorption lines in the 2.7-μm band of CO_2. In the LDD examined here, the pressure in the energy addition region is about 6 - 7 atm. Thus, there will be significant pressure broadening of the absorption lines, and energy transfer from the laser beam to the vibrational modes of CO_2 will be effective. The laser beams are surmised to have their maximum transfer of energy to the gas in the relatively high-pressure region near the exit of the slowly varying section at an axial position of about 20 cm. The

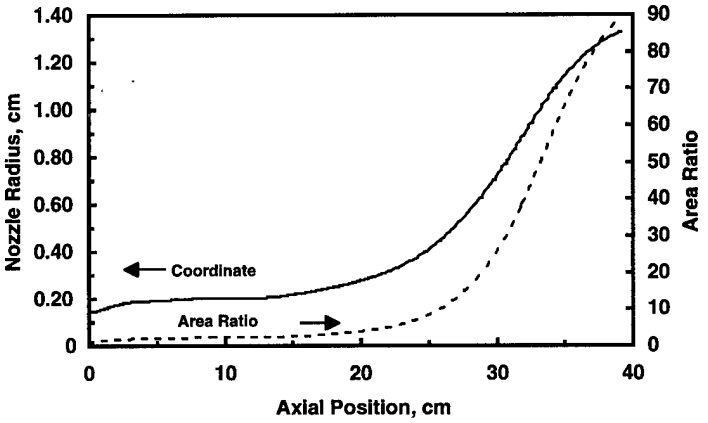

Fig. 1. Nozzle contour.

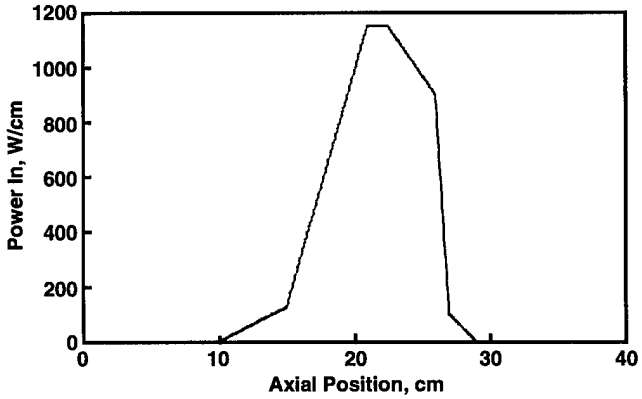

Fig. 2. Power addition profile.

region from about 10 to 15 cm serves as a high-pressure region that absorbs the remainder of the energy not absorbed further downstream.[1]

Molecular Model

Critical to the understanding of the thermalization of the energy that will be added to the flow of the RDHWT is the understanding of the distribution of the internal energy states of the molecules participating in the thermalization. Nitrogen and O_2 are diatomic molecules with relatively simple vibrational structure, while CO_2 is a triatomic molecule with a more complicated structure. It is, however, a linear molecule and, consequently, there are regularities in the term structure that simplify modeling.

A partial term diagram for CO_2 is shown in Fig. 3. Only the $v_3 = 0$ levels through $v_1 = 4$ and $v_2 = 8$ are shown. States from the other series, $v_3 = 1$ and $v_3 = 2$, are included in the flow calculations and are included in the discussion below, but this partial term diagram will be used to explain the complexity of the CO_2 molecule and the simplifying assumptions used here. The numbers in parentheses below each line in the CO_2 portion of the term diagram are the v_1, v_2', and v_3 (symmetric stretch, bending, and asymmetric stretch) quantum numbers, respectively. The well-known attribute of CO_2, the "accidental" degeneracy, or Fermi resonance,[7] in the v_1 and v_2 modes (every second v_2 is in near resonance with a v_1), is apparent in Fig. 3. These states (e.g., (10^00), (02^00)), are close together energetically, and there is, in a quantum mechanical sense, a mixing of the wave functions of these states. Pragmatically, these states are virtually indistinguishable and it is very easy to maintain an LTE distribution of densities among these states that exhibit this Fermi resonance.

The CO_2 states that exhibit this resonance and close energy coupling, e.g., the (06^60), (06^40), ($1,4^40$), (06^20), (14^20), (22^20), (06^00), (14^00), (22^00), and (30^00) states at about 4,000 cm^{-1}, are grouped together and are treated as a single state for this work. They are designated with a capital L in the notation, e.g., (06L0). Those states in this grouping that are not connected through the Fermi resonance are very close together energetically and, as will be seen in a discussion of the rate coefficients, can be expected to exhibit a thermal distribution among themselves. Grouping the states in this manner reduces the number of individual states included on the flow calculation to a manageable number without sacrificing the essential physics necessary to investigate the details of the thermalization of the input laser power. There is similar structure with each v_3 value ($v_3 = 2$ was the highest included here), and the grouping of the v_1 and v_2 states for each v_3 was accomplished.

Figure 4 shows the resulting term diagram that was used for the calculations here, including the N_2 and O_2 vibrational states. For the CO_2 modes there are additional upper states designated "U0," "U1," and "U2." Included in each of these states are the states between the highest individual state considered and the U state for $v_3 = 0$, 1, and 2, respectively. These states are connected collisionally to

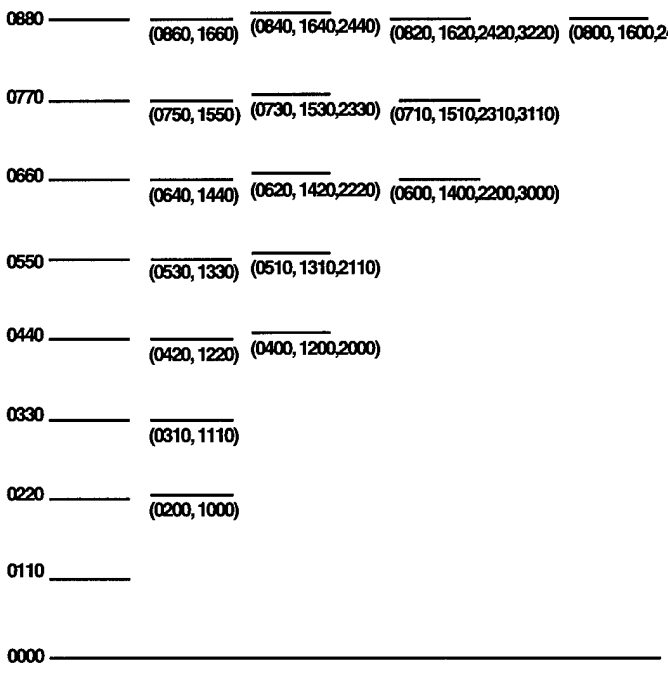

Fig. 3. CO_2 $v_3 = 0$ term diagram.

the highest individual state for each ν_3 with a collision number of 10. Included also are a number of states with a "U" in their designation. These represent manifolds of states above the energy at which individual states (or collection of states) were kept distinct. Included in the "U" states for each molecule are all the states higher than 10,000 cm^{-1} . These states provide a reservoir of upper states that are connected to the next lower states through simple thermal collisions with a collision number of 10,000. These states thus provide a reservoir to include the rest of the molecular states necessary for completeness and connect them to the lower states in a manner that is physically consistent with observations. With these considerations, it is seen that the modeling includes 23 distinct states of CO_2, 5 of N_2, and 5 of O_2.

It is seen in Fig. 4 that the states of N_2 are in near resonance with the $(00^0\nu_3)$ modes of CO_2, whereas the excited states of O_2 are at somewhat lower energies than either the N_2 or CO_2. The N_2 - CO_2 and N_2 - O_2 V-V transitions are a well-known pathway for the de-excitation of CO_2 and N_2. Inclusion of these states is an important path for the thermalization of the input energy, since the N_2 will provide a path for energy transfer from the CO_2 ν_3 excited modes, and the O_2 will then provide a path for the de-excitation of the N_2.

The transition for the laser absorption in also shown in Fig. 4. The proposed LDD will deposit energy into the flow through several laser lines

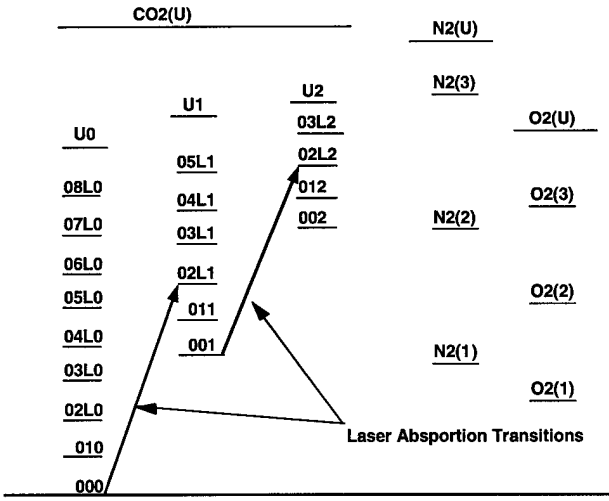

Fig. 4. Species term diagram.

between about 3,500 cm^{-1} and 3,700 cm^{-1}. These lines are in the spectral region for several absorption lines from the CO_2 ground states and the (10^01)-(02^l1) states, which are in the (02L1) state. Although the laser lines are very narrow and a Doppler shift of the absorbing lines may be significant, absorption occurs in the higher pressure portions of the flow where the rotational lines are pressure broadened. It should be noted that there will be an additional absorption transition from the (001) state to the (02L2) state, the (002) to the (02L3) state, and so on. Any final modeling of the radiative heating will have to include these transitions as well.

Flow Solver

As in the earlier work[5,6,8-10] the One Dimensional Kinetic (ODK) code[11] is used as the flow solver for this calculation. The ODK code calculates the inviscid, chemically reacting nozzle expansions of gaseous exhaust mixtures. The specific version used here was included as a subprogram to the larger Two-Dimensional Kinetic Analysis Program (TDK)[12] and allowed up to 150 chemical reactions and 40 species. A modified version of the NASA Equilibrium code[13] is also included as a subprogram of the larger TDK code. A complete description of the codes is included in the TDK manual.[12] The results of the equilibrium code for the combustion chamber are used as initial values at a specified initial contraction ratio. The flow is described by using a defined pressure distribution from the combustion chamber to the sonic point and geometry-defined relations through the supersonic portion. The pressure distribution for the subsonic flow is obtained from the equilibrium solution. The species production equations from the chemistry are coupled to the gas-dynamic equations in the conventional way. The resulting differential equations are integrated by a second-order implicit method derived in Nickerson, et al.[12] Step-size control is included to ensure that the rates of change of the sundry gas-dynamic, species production, and energy production terms are maintained within the form of the solution implied by the second order numerical technique used.

In principle, there is no requirement that the species be distinct chemical species. Treating each excited vibrational state as a separate species allows one to calculate the development of the state densities in an expanding flow. All that is required for calculation are the appropriate rate coefficients and the appropriate thermodynamics for the molecular internal distributions chosen. With these physical properties, the conventional finite-rate chemistry gas-dynamic code can be used to calculate the internal distribution of states as the gas flow develops along the nozzle as if each state were a separate chemical specie. A separately defined vibrational temperature for the description of the internal distribution function is unnecessary. In this manner, a non-Boltzmann vibrational distribution will manifest itself as a natural result of the calculation when the collision frequency becomes too low to maintain a particular state in collisional equilibrium with the rest of the ensemble. This is the approach taken here and the details of the molecular model and thermodynamics used for this calculation are described below.

Thermodynamics

The flow code used[11-12] requires curve fits in the NASA form[13] for the species nondimensional enthalpy, H/RT, specific heat, C_p/R, and entropy, S/R. These quantities are defined for an ensemble gas at thermal equilibrium and include the contributions of each of the states considered here. Since the molecular approach here is to treat each separate collection of molecular states as a separate species, it was necessary to generate curve-fit coefficients for each of the collections considered.

This was accomplished with the specific heat, enthalpy, and entropy defined from the partition functions in the usual way.[14]

$$\frac{C_p}{R} = \frac{5}{2} + \frac{d}{dT}\left(T^2 \frac{d\,ln Q_{int}}{dT}\right)$$

$$\frac{H}{RT} = \frac{5}{2} + \frac{G(v_0)}{RT} + T\frac{d\,ln Q_{int}}{dT}$$

$$\frac{S}{R} = \frac{S_{tr}}{R} + ln Q_{int} + T\frac{d\,ln Q_{int}}{dT}$$

where

$$\frac{S_{tr}}{T} = 1.1512(5\log_{10}T + 3\log_{10}M) - 1.1647$$

and M is the molecular weight, T is the temperature, and $G(v_0)$ is the reference zero point energy for the manifold. The internal partition functions are calculated only over those specific vibrational states comprising the particular manifold:

$$Q_{int} = \sum_{v_0}^{v_{max}} Q_{r_v}(T) g_v e^{-\frac{G(v) - G(v_0)}{kT}}$$

Although the rotational states are assumed to be in thermal equilibrium at the gas temperature, the rotational partition function was calculated for each vibrational state. The molecular constants for the molecular potential functions were taken from Ref. 15 for the diatomic molecules N_2 and O_2 and Ref. 16 for CO_2. Since the rotational constant, B_v, and the centrifugal constant, D_e, may be different for each of the different stretching and bending modes, they were calculated for each level.

The thermodynamic properties for each collection of states were calculated in 100 K increments from 200 to 3,000 K and the results least square curve fit to the functional form of the NASA coefficients. Two sets of coefficients were generated, one set for temperatures below 1,000 K and the other set for the temperature range from 1,000 K to 3,000 K. The curve fits were generated over both temperature ranges simultaneously and were constrained to be continuous and smooth at 1,000 K.

RATE COEFFICIENTS

The molecular model for CO_2 required for this study included significantly higher vibrational states than had been included in previous work (e.g., Ref. 6), and a different distribution of individual microstates within each discrete collection was used for the computation. Consequently, it was necessary to review the rate coefficients used previously for application to the present problem. Fortunately, considerable experimental work was performed on the state-specific relaxation rates of CO_2 during the late 1960's and early 1970's and significant compilations of rates exist.[17-18] The measurements of that era concentrated on the

states in the ν_3 = 0 manifold, ranging from the ground state to (05^50), and there has been little work in this area since. Accurate modeling of the CO_2 relaxation in the RDHWT depends greatly upon energy transfer between very highly excited vibrational states, including those much higher than (05^50) and other ν_3 manifolds. Thus, it was necessary to define a method of incorporating measured energy transfer rates where available, and generate reliable reaction rates for unmeasured processes.

Figure 5 shows a small portion of the CO_2 term diagram of Fig. 3 and includes some of the detailed states of the ν_3 manifold. Denoted in Fig. 5 are the transitions in which the rate was either measured (solid line) or theoretically calculated (dashed line). As mentioned above, the measured rate data is complete for all transitions shown, including the ground state through the (05^50). To determine the VT rates for the other upper states required here, an extrapolation procedure was developed which was based upon the separability of the dynamic collision process from the quantum mechanical probability for transition between eigenstates. The set of VT reactions can be broken into subsets, in which each subset is composed of those relaxation reactions which undergo a specified change in vibrational quanta. Since the collision dynamics are a consequence of the inelasticity of the collision, each reaction of a given subset will have identical collisional behavior because of the identical change in energy and angular momentum. Hence, VT reactions of upper states can be scaled from lower states within the same subset with an identical temperature dependence as the lower state. This crucial assumption then alleviates the need for detailed first-principle calculations of velocity-dependent, state-specific, collision cross sections for the large number of upper CO_2 states. The variation of the VT rate for reactions within a given subset will behave as the variation of the transition matrix element, which is a function of the initial set of vibrational quantum numbers. Nineteen subsets of reactions with defined vibrational quanta changes were identified in this analysis.

The calculation of the transition matrix must consider the Fermi resonance of the ν_1 and ν_2 modes. This accidental degeneracy leads to a mixing of states of similar symmetry and the resultant state is denoted by parentheses enclosing all degenerate states. For example, the degenerate states (02^00, 10^00) are written, to first order, as [7]

$$(02^00, 10^00) = 0.73\ |\ 02^00\rangle + 0.68\ |\ 10^00\rangle$$

and

$$(02^00, 10^00) = -0.68\ |\ 02^00\rangle + 0.73\ |10^00\rangle$$

The state expansions are important in the calculation of the transition matrix elements between states since the coupling coefficients lead to additional nonzero transition elements due to the cross terms of the interaction Hamiltonian. For the upper states of the ν_3 manifolds, the degree of the Fermi degeneracy increases, such as for the (08^20, 16^20, 24^20, 32^20) state. Thus, relaxation of this state into the (07^30, 15^30, 23^30) can invoke numerous cross terms. In this analysis, the eigenstates were com-

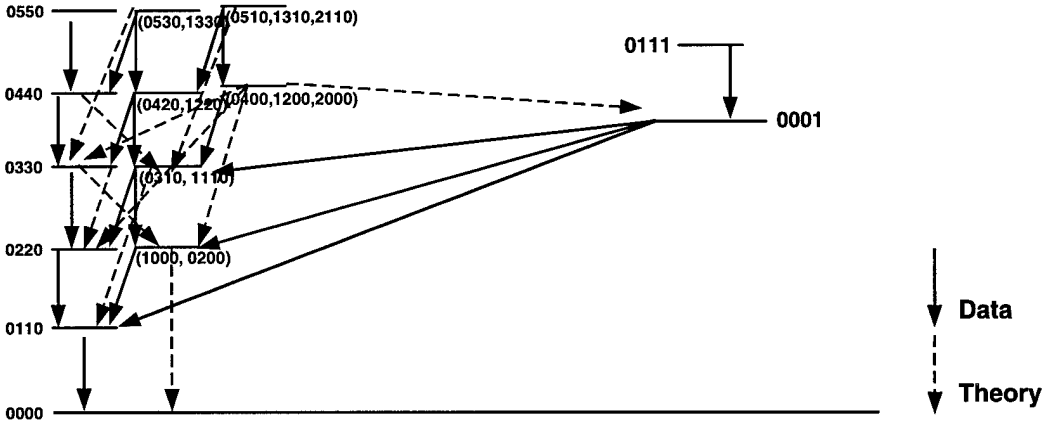

Fig. 5. Existing rate constants for CO2 VT reactions.

puted to second order in order to capture the third-order interaction amplitude. This degree of expansion proved especially useful when incorporating relaxation transitions involving the v3 mode.

As an example of the rate scaling methodology, consider two subsets of relaxation as denoted on Fig. 6, denoted as Group I and Group II. In Group I, the set of relaxation processes is characterized by the change of spectroscopic quantum numbers $(0\ n^{n-2}\ 0,\ 1\ n\text{-}2^{n-2}\ 0) \rightarrow (0\ n\text{-}1^{n-3}\ 0,\ 1\ n\text{-}3^{n-3}\ 0)$. Note that for this subset of relaxation reactions, three reactions were measured,

$(03^10, 11^10) \rightarrow (02^00, 10^00)$,

$(04^20, 12^20) \rightarrow (03^10, 11^10)$,

$(05^30, 13^30) \rightarrow (04^20, 12^20)$,

as indicated by the solid lines in Fig. 6. The rates were tabulated in the standard Landau format, $lnk = A + B/T + CT^{1/3}$, in Ref. 18. Figure 7 shows the value of the parameter A for these three reactions. Also shown in this figure is the extrapolation of the relaxation rate parameter A for relaxation of higher vibrational states of the same subset. The variation of the A parameter is well modeled for those rates where measured data exists, remembering, of course, that one rate, in this case the lowest rate, was used to scale the absolute magnitude of the extrapolation.

The Group I rates shown in Fig. 6 are dominated by the first-order term in the interaction amplitude, i.e., the change of only one vibrational quanta. The more complicated Group II transitions, which involve v_3 mode transitions, require second- and third-order terms for correct physical representation, i.e., v_1 and v_2 transitions as well. Since the computation of the third-order terms required insignificant additional effort, all reaction rates were eventually calculated to this order, regardless of the magnitude of the third-order term relative to the lower-order terms.

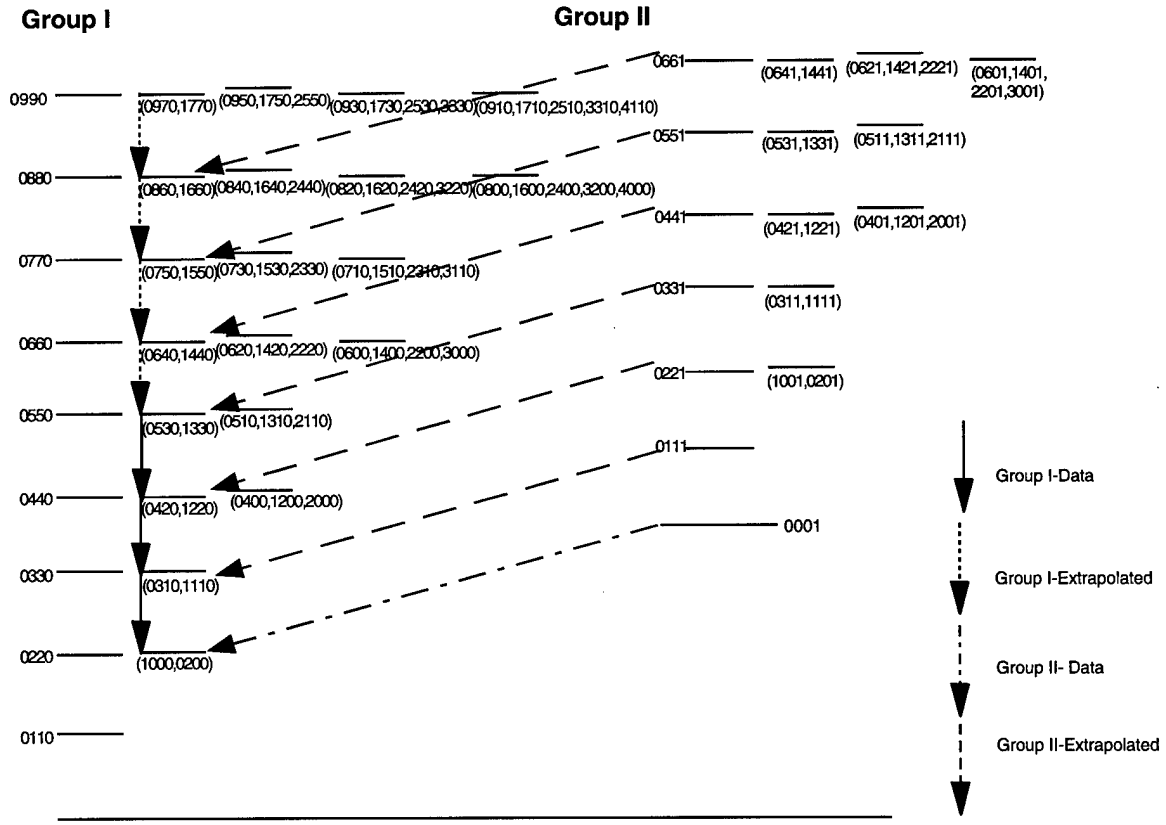

Fig. 6. Example extrapolation groups.

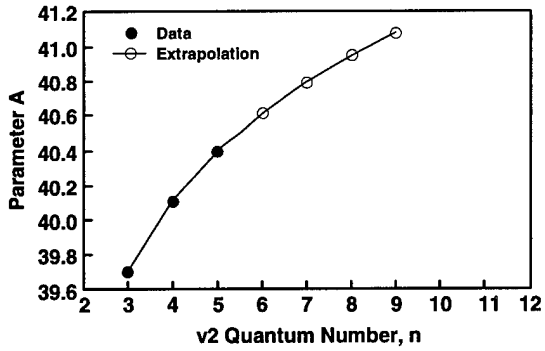

Fig. 7. Data and extrapolated rate constants, A, for Group 1 reactions of Fig. 6.

With the state-specific relaxation rates extrapolated from the measured data for almost all the rates of interest, some method of reducing the number of total CO_2 states to coincide with the LDD modeling was necessary. With the collecting of the individual microstates into a single state described above, the final issue is to determine the proper combination of state-specific rates that describes the relation between macrostate relaxation.

Consider a macrostate N, defined by a certain combination of true states. The number density of the macrostate, N_T, is then the sum of the number densities of the true states, N_i. The time variation of the true state densities may be given as,

$$\frac{dN_i}{dt} \equiv \dot{N}_i \equiv -\sum_j k_{ij}^{out} N_i X + \sum_j k_{ij}^{in} M_j X$$
$$= X\sum_j \left(k_{ij}^{in} M_j - k_{ij}^{out} N_i \right)$$

where X denotes the arbitrary collision partner and M_i denotes states from macrostate M which relax into macrostate N. The rate of change of the density of the entire macrostate follows as

$$\dot{N}_T = \sum_i \dot{N}_i$$
$$= X\sum_j M_j \sum_i k_{ij}^{in} - \sum_i N_i \sum_j k^{out}_{ij}$$
$$= X\left(K^I_{MN} M_T - K^O_N N_T \right)$$

where the final line serves as a definition. To allow for the macrostate rate solution, an assumption is made that the densities of the true states within a macrostate are defined by thermal equilibrium. This is reasonable if the energy differences between the states are small, and constitutes the driving rule-of-thumb for macrostate definition. In this instance, the macrostate rate can then be written as

$$K^I_{MN} = \frac{1}{M_T}\sum_j M_j \sum_i k_{ij}^{in} = \sum_j \frac{g_j e^{\frac{-E_j^M}{kT}}}{Q_M(T)} \sum_i k_{ij}^{M \to N}$$

where $Q_M(T)$ denotes the partition function taken over the M macrostate. Thus, the net relaxation rate between macrostates can be written as a properly averaged sum of the state-specific relaxation rates between all the components of the two macrostates. This computation was carried out for the 19 VT macrostate relaxation processes used in the flow computation.

Results

The gas dynamic results of the calculations are shown in Figs. 8 - 10. Figure 8 is the Mach number, Fig. 9 is the static temperature, and Fig. 10 is the static pressure. Results of four calculations are included on each figure:

1. An LTE calculation with no heat addition

2. A LTE calculation with heat addition

3. A state specific relaxation (SRR) calculation with no heat addition

4. An SSR calculation with heat addition

Additionally, on Fig. 9, the static temperature for a calculation in which the 10-kW input power was added to the plenum chamber rather than in the downstream supersonic portion, is shown. On the scale of these figures, there is no discernible difference between the LTE and SSR calculations when there is no energy addition in the supersonic stream. Hence, the lines corresponding to calculations 1 and 2 above are indistinguishable. The LTE calculations were accomplished with the same state reactions used for the SSR calculations, except with the rate coefficients increased to thermal rates. That is, the rate coefficient is increased so that every molecular collision results in a transition. Included also on each of the figures is a nor-

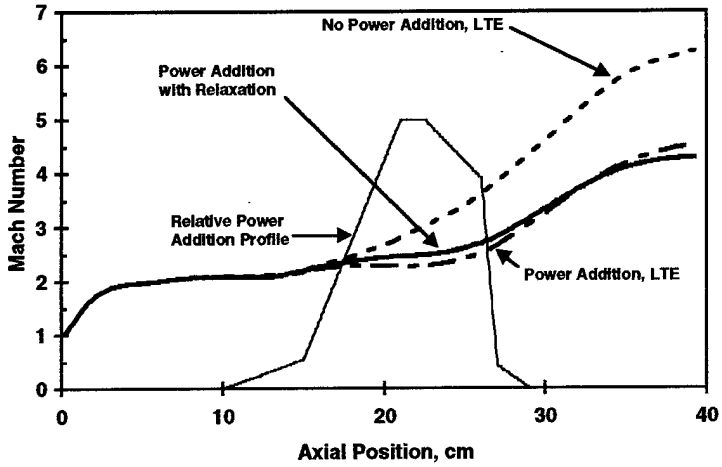

Fig. 8. Mach number axial profiles.

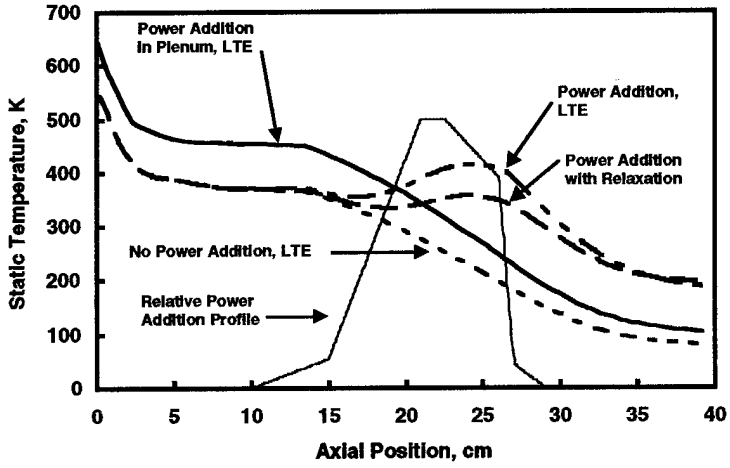

Fig. 9. Static temperature axial profiles.

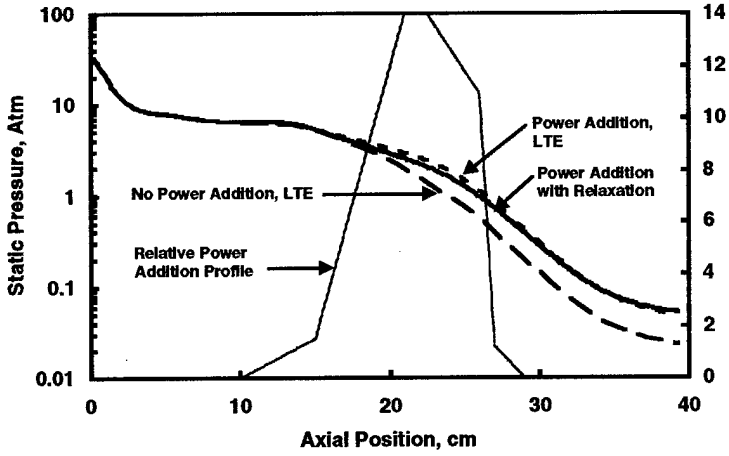

Fig. 10. Static pressure axial profiles.

malized energy addition profile (Fig. 2) for easy reference.

Clearly, the energy addition and the vibrational relaxation has an effect on the flow. Examining Fig. 9, it is seen that adding the energy to the plenum chamber results in an increase in the LTE exit plane temperature of about 25 K above the LTE with no heat addition. There are attendant changes in Mach number, velocity, temperature, etc. For the calculations in which the power input is downstream of the throat, all calculated properties are coincident upstream of the energy addition. Shortly downstream of the point at which the energy addition commences, the SSR and LTE calculations begin to show deviations from the baseline curve. For the region of energy addition, the LTE calculation shows a higher temperature and lower Mach number than the SSR calculation, as one would expect. Since the LTE calculation thermalizes the input energy almost immediately, that energy is available for heating of the flow. In the case of the SSR, the input energy is maintained in the internal distribution and is not released to the gas until further downstream. Interestingly, at the exit plane, the LTE calculation shows higher Mach number and lower temperature than the SSR, indicating that there is still significant energy stored in the vibrational distribution of the molecules. The static pressure shows similar characteristics, with the LTE calculation showing the greatest increase above the baseline calculation and the SSR and LTE calculation crossing near the exit plane.

Because there is a demonstrable difference at the exit plane between the SSR and LTE calculations, it is of interest to examine the internal energy distribution determined by the SSR calculation. This is shown in the form of Boltzmann plots (Figs. 11 and 12) of the

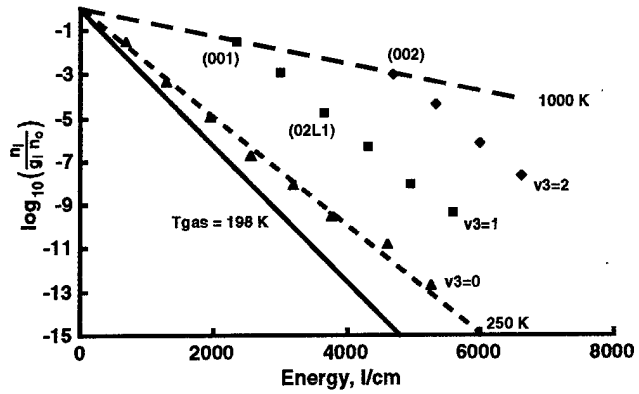

Fig. 11. Exit plane Boltzmann plot of CO_2 internal state densities.

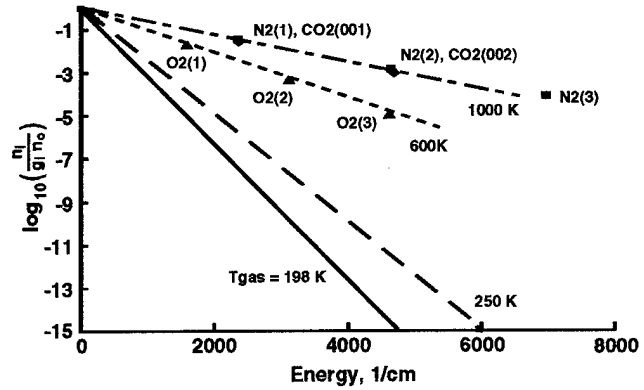

Fig. 12. Exit plane Boltzmann plot of selected CO_2, N_2, and O_2 densities.

excited species at the exit plane. The ordinate is the logarithm (base 10) of the number density of the specific vibrational state relative to the statistical weight and the ground-state density, and the abscissa is the internal energy. On a plot of this nature, those states that are in thermal equilibrium with each other lie on the same straight line at a slope of (–1/kT) where k is Boltzmann's constant and T is the temperature of the distribution.

Figure 11 shows the Boltzmann plot at the exit plane of the CO_2 internal states only and the NLTE nature of the distribution is evident. Each state included for CO_2 is shown except for the artificial upper manifolds of states. Examining the detailed states plotted, clearly there is no single straight line that can be used to characterize the CO_2 vibrational distribution. There are some apparent relationships between collections of states that are worth examining and there are three lines drawn on the figure to illustrate these relationships. It is emphasized that the only temperature used throughout the calculations was the gas translational temperature, and it is shown and identified on the plot as T_{gas} = 198K. The states with specific ν_3 appear to fall on the straight line at some other temperature. This is illustrated on the figure by a line drawn through the states with ν_3 = 0. This equivalent temperature is at 250 K, and is significantly different than the gas temperature. Although nearly at the same slope, the distributions for the series of states ν_3 = 1, 2 appear to be at a slightly different temperatures compared to each other and to the ν_3 = 0 series. This difference in slope may easily be a manifestation of the effect of the assumptions about the upper states and their coupling to the next lower state. If enough states were included in each manifold, the temperature characteristic of the distribution of states within each manifold might easily be the same. The lowest states in each of the ν_3 manifolds appear to fall on the same straight line also, albeit there are only three states to determine this. The apparent equivalent temperature for this relationship is 1,000 K. Clearly, a description of the CO_2 internal distribution will require accounting for at least three temperatures.

Figure 12 shows an exit plane Boltzmann plot including the N_2 and O_2 vibrational states but including only the CO_2 (000), (001), and (002) states. The lines at the temperatures 250K and 1,000 K are shown for easy reference. The strong coupling between the states of N_2, and the ν_3 modes of CO_2 is evident. The N_2 vibrational states nearly overlay the (001) and (002) states of CO_2 and appear to exhibit the same distribution, as evidenced by the straight line at 1,000 K drawn through those densities. The O_2 vibrational states, however, exhibit a different relationship which has a lower characteristic temperature, here about 600 K. This is a consequence of the N_2 - O_2 V-V relaxation rate and the V-T relaxation of O_2 being at different characteristic rates than the N_2 - CO_2 V-V and V-T relaxation.

Examination of Boltzmann plots at different axial positions shows essentially the same results, with the ν_3 manifolds of CO_2 exhibiting a tempera-

ture above the gas translational temperature, the N_2 and $CO_2(00v_3)$ exhibiting another temperature, and the O_2 exhibiting yet another. It appears that, for accurate description of the energy deposition and the relaxation of the molecules, at least four temperatures will be necessary. It is notable that the CO_2(02L1) state, which absorbs all the energy of the beam, does not show significant departures from the distribution with its neighboring states with the same v_3, even in the axial region of greatest power addition. It should be noted that there is in fact an elevation of this state above the distribution, but it is not discernible on plots of this scale. This implies that the thermalization of the energy into the adjacent states is in fact quite rapid, and the (02L1) state never shows a great departure from its instantaneous internal distribution which is determined by the relaxation of CO_2 as a whole.

It is instructive to examine the relative mole fraction of several of the states important in the relaxation process. This is shown in Fig. 13, which shows the axial profiles of the relative mole fractions of the (000) ground state, the (02L1) state which is pumped by the laser, and the (001) state, the lowest state in the manifold including the (02L1) state. The molecular mole fractions have been normalized by their maximum value so that relative comparisons can be made. Here it can be seen that the (02L1) state shows a very rapid increase in mole fraction with the heating profile increase. At the same time, since the laser is pumping molecules from the ground (000) state to the (02L1) state, the (000) state shows a slight decrease. The relative changes in the two curves is significantly different because there are about four orders of magnitude more molecules in the ground state than in the (02L1) state. The (02L1) state continues to increase in mole fraction until about 25 cm, at which there is rapid decay consistent with the assumed decrease in energy deposition from the laser beam. The (001) state, which is connected only collisionally to the (02L1) state through the rate coefficients, shows an increase similar to the (02L1) state, albeit lagging slightly, Downstream of the heating profile the (001) and (02L1) states appear to decay exponentially, reflecting the deactivation of the species and the transfer of the internal energy into the translational temperature. The (000) state, however, shows an increase in mole fraction as all the molecules that were pumped into higher states decay back down.

It is of interest to examine the energy content of the vibrational distribution relative to the energy input to the gas and included in the excited distribution. This is shown in Fig. 14. Three results curves are shown on Fig. 14 in addition to the relative energy addition profile. Two of the curves illustrate the total power injected into the (02L1) state by the laser and the power carried in the excited NLTE internal energy states in excess of that in the LTE distribution, respectively. These curves use the right ordinate. The other curve is the fractional portion of the input power that is stored in the NLTE distribution beyond the LTE content of the excited states and uses the left ordinate. The power in the excited NLTE distribution is determined by simply adding up the number of molecules in each state multiplied by the energy of that state and dividing by the instantaneous velocity and area. The power in the LTE distribution is arrived at the same way, except that the population density of each state is calculated from the Boltzmann distribution at the instantaneous gas static temperature. The total power injected into the (02L1) state is simply the integral of the energy addition profile shown in Fig. 2.

Some interesting observations arise from Fig. 14. First, note that the energy content in the NLTE distribution rises with the input power to an axial

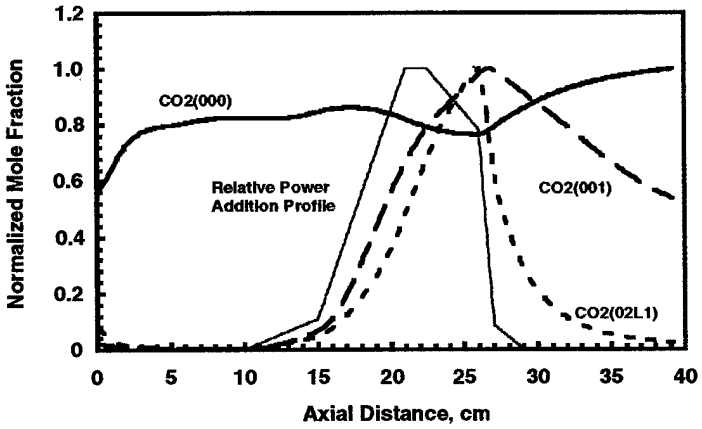

Fig. 13. Mole fractions axial profiles.

position of about 25 cm, at which point the energy deposited into the gas drops sharply. At that point collisional processes dominate the radiative excitation process and there is a decrease in the power content in the NLTE distribution. This is consistent with physical intuition, realizing that the process of energy redistribution to the other modes of the gas require finite times to accomplish whereas there is an instantaneous perturbation in the excited state distribution because of the laser absorption. The plot of the excess power in the NLTE distribution relative to the total power input shows an almost instantaneous increase to near 90 percent at an axial position of about 10 cm, the point at which energy addition commences in the flowing gas. The relative power then starts to decay slightly to an axial position of about 15 cm at which it again increases to near 87 percent. The 15-cm axial position marks a point at which the rate of energy deposition into the (02L1) state increases significantly. Near 10 cm, the instantaneous population of the (02L1) state becomes relatively large enough that the collisional depopulating processes become competitive with the rate of the populating laser input. Between 10 and 15 cm, since the rate of energy input is constant, the collisional processes come to dominate the NLTE distribution and the relative power in the NLTE distribution decreases. When the rate of laser power input increases at 15 cm, the radiative process again dominates the collisional for a short time, and the power in the NLTE distribution again increases. From this point, since the rate of power input doesn't increase again, the relative power in the NLTE distribution continues to decrease. At an axial position of about 25 cm, the rate of laser power into the gas has a sharp decrease and the decay characteristic of the NLTE distribution increases. Significantly, for this nozzle, there is still about 19 percent (note the left-hand scale) of the input laser power that is still contained in the NLTE distribution at the nozzle exit. A longer nozzle will allow still more of the energy to be converted to the kinetic modes of the gas and allow larger Mach numbers at the nozzle exit.

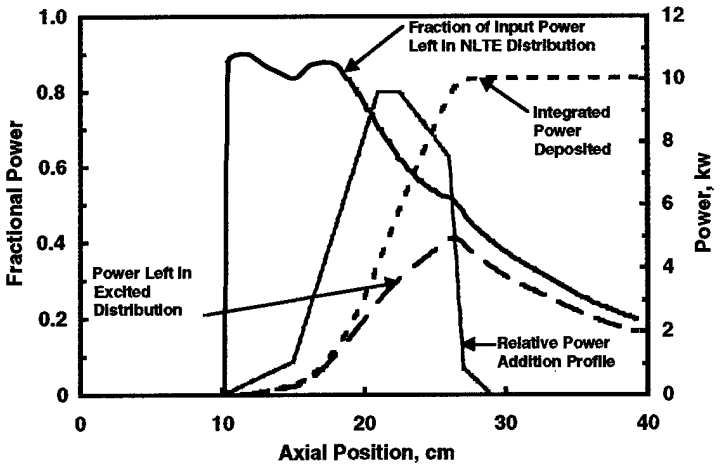

Fig. 14. Power in NLTE distribution calculated from SSR model.

Summary

State-specific relaxation (SSR) calculations for a demonstration experiment intended to show efficacy of the radiatively heated wind tunnel (RDHWT) concept were accomplished. The RDHWT is a one of several proposed methods to add energy into the supersonic portion of a nozzle flow to increase the test chamber conditions (static temperature, Mach number, etc.) to hypersonic flight conditions. Material limitations in current wind tunnel technology preclude test times of more than a few milliseconds duration and with air compositions representative of flight. Adding energy into the supersonic portion provides the opportunity to increase the energy of the flow while still staying within material limits. The key to successful wind tunnel design will be the ability to predict and control the energy input and the expansion to achieve *a priori* test conditions. To this end, a demonstration experiment has been proposed to test the ability to add the energy in the supersonic flow with predictable results.[7]

The demonstration model investigated operates at much lower pressures and laser powers than the full-scale facility, but suffices to demonstrate the heating of supersonic air in a predictable and controllable manner. The working gas for the demonstration calculations were air seeded to a 40-percent concentration of CO_2. The laser used was a

10-kW HF laser which will couple to the CO_2 in the flow, pumping the ground state of CO_2 to the $(02^{l}1)$ state. Plenum pressure was about 100 atm and temperature was 1,150 K.

The SSR model treats each vibrational level of the gas molecules as a separate species and does not depend upon any of the usual assumptions regarding the distribution of the energy internal to the molecular structure. With this approach, the input laser energy can pump a specific vibrational state (as it will in an experiment) and the relaxation from that specific state through the rest of the distribution to the translational modes of the gas can be examined.

Results of the calculations show that, at the conditions used, most of the deposited energy is thermalized into the flow. The relaxation has an effect, in that compared to a thermal equilibrium calculation, there was still significant energy bound in the excited NLTE internal distribution at the exit plane. Longer nozzles and slower expansions will allow greater thermalization of the input power. The relaxing distribution of internal vibrational states of the flow molecules exhibited definite non-Boltzmann distributions, although states with certain excitation characteristics did exhibit thermal-like characteristics, albeit at temperatures other than the gas translational temperature. For CO_2 the $(00v_3)$ states appear to exhibit one temperature distribution while the states with constant v_3 exhibit a different temperature distribution. The CO_2 $(00v_3)$ and the $N_2(v)$ states exhibit their well-known strong coupling and manifest the same thermal-like relationship. The $O_2(v)$ states also appear to exhibit thermal-like characteristics, but at yet another temperature. Correct accounting of the energy content of the vibrationally relaxing flow will have to include these different temperature-like characteristics, since significant energy can be stored in each of the different modes, and the details of the release of the stored energy to the flow will affect the calculation of the exit plane properties.

References

1. Miles, R. B., et al. "Radiatively Driven Hypersonic Wind Tunnel." *AIAA Journal*, Vol. 33. No. 8, August 1995, pp. 1463 - 1470.

2. Macheret, S., et al. "Energy Addition and Thermalization Issues in a Radiatively Driven Hypersonic Wind Tunnel." AIAA-95-2142, 30th AIAA Thermophysics Conference, San Diego, CA, June 19-22, 1995.

3. Macheret, S., et al. "Radiative Energy Addition to High Pressure Supersonic Air." AIAA-96-1984, 27th AIAA Fluid Dynamics Conference, New Orleans, LA, June 17-20, 1996.

4. Brown, G. L., et al. "Fluid Mechanics in a Radiatively Driven Hypersonic Wind Tunnel - Prediction and Experiment." AIAA-96-2199, 19th AIAA Advanced Measurement and Ground Testing Technology Conference, New Orleans, LA, June 17 - 20, 1996.

5. Limbaugh, C. C. "Gas Diagnostics for High Area Ratio Rockets." AIAA-85-1082. AIAA 20th Thermophysics conference, Williamsburgh, VA, June 19-21, 1985.

6. Limbaugh, C. C., Tramel, R. W., Drakes, J. A., and Hiers III, R. S. "Analysis of CO_2 Vibronic Ensembles in Nonequilibrium Combustion Flows." AIAA-94-1985, 6th AIAA/ASME Joint Thermophysics and Heat Transfer Conference, Colorado Springs, CO, June 20-23, 1994.

7. Herzfeld, K. F. "Deactivation of Vibrations by Collision in the Presence of Fermi Resonance." *Journal of Chemical Physics*, Vol. 47, No. 2, July 15, 1967, pp. 643 - 752.

8. Limbaugh, C. C., Hiers III, R. S., and Phillips, W. J. "High-Resolution Diagnostics on Flows with Mild Vibrational Relaxation." AIAA Paper No. AIAA-89-1676, AIAA 24th Thermophysics Conference, Buffalo, NY, June 12-14, 1989.

9. Limbaugh, C. C., Hiers III, R. S., and Phillips, W. J. "Spectral Radiative Transfer for the 4.0- to 5.0-μm Bands of CO_2 With Mild Vibrational Relaxation and Doppler Shift." AIAA-90-1782, AIAA/ASME Joint Thermophysics and Heat Transfer Conference, Seattle, WA. June 18 - 20,1990.

10. Limbaugh, C. C. and Drakes, J. A. "Validations of Doppler Shift Effects for Infrared Band

Model Calculations." AIAA-91-1430 AIAA 26th Thermophysics Conference, Honolulu, HI, June 24-26, 1991.

11. Frey, H. M., Nickerson, G. R., and Tyson, T. J. "One Dimensional Kinetic Analysis Reference Computer Program." Dynamic Science Report No. CS-1-9/70, September 1970.

12. Nickerson, G. R., Coates, D. E., and Bartz, J. L. "Engineering and Programming Manual, Two Dimensional Kinetic (TDK) Reference Computer Program." NASA-CR-152999, December 1973.

13. Mc Bride, B. J. and Gordon, S. "Computer Program for Calculating and Fitting Thermodynamic Functions." NASA Reference Publication 1271, Lewis Research Center, Cleveland, OH, 1992.

14. Herzberg, G. *Molecular Spectra and Molecular Structure: Volume II. Infrared and Raman Spectra of Polyatomic Molecules.* van Nostrand, Princeton, 1945.

15. Herzberg, G. and Huber, K. P. *Molecular Spectra and Molecular Structure: Volume IV. Constants of Diatomic Molecules.* van Nostrand Reinhold, New York, 1979.

16. Rothman, L. S., and Young, L. D. G. "Infrared Energy Levels of Carbon Dioxide-II". *Journal of Quantitative Spectroscopy and Radiative Transfer,* Vol. 25, 1981, pp. 505-524.

17. Taylor, R. L. and Bitterman, S. "Survey of Vibrational Relaxation Data for Processes Important in the CO_2-N_2 Laser System." *Reviews of Modern Physics,* Vol 41, No. 1, January 1969, pp. 26-47.

18. Blauer, J. A. and Nickerson, G. R. "A Survey of Vibrational Relaxation Rate Data for Processes Important to CO_2-N_2-H_2O Infrared Plume Radiation." AIAA Paper No. 74-536, AIAA 7th Fluid and Plasma Dynamics Conference, Palo Alto, CA, June 1-19, 1974.

REPORT DOCUMENTATION PAGE

Form Approved
OMB No. 0704-0188

1. AGENCY USE ONLY *(Leave blank)*	2. REPORT DATE	3. REPORT TYPE AND DATES COVERED
	June 1997	Technical Society Paper

4. TITLE AND SUBTITLE
CO 2 Vibrational Relaxation Effects in a Laser-Heated Hypersonic Flow
AIAA Paper No. 97-2492

5. FUNDING NUMBERS
Project 3220

6. AUTHOR(S)
C. C. Limbaugh and J. A. Drakes

7. PERFORMING ORGANIZATION NAME(S) AND ADDRESS(ES)
Sverdrup Technology, Inc., AEDC Group
Arnold Engineering Development Center
Arnold AFB, TN 37388

8. PERFORMING ORGANIZATION REPORT NUMBER

9. SPONSORING/MONITORING AGENCY NAME(S) AND ADDRESS(ES)
Arnold Engineering Development Center
Arnold AFB, TN 37388

10. SPONSORING/MONITORING AGENCY REPORT NUMBER

11. SUPPLEMENTARY NOTES
Presented at 32nd Thermophysics Conference in Atlanta, GA.

12a. DISTRIBUTION AVAILABILITY STATEMENT
Approved for public release; distribution unlimited.

12b. DISTRIBUTION CODE
A

13. ABSTRACT *(Maximum 200 words)*

The establishment of flow conditions characteristic of hypersonic flight in a ground test facility by conventional means requires plenum conditions that have very high temperatures and give rise to a variety of materials problems. A well-known approach to solving theseproblems is to use high-pressure, moderate temperature plenum condi-tions and add energy as the flow expands through a carefully designed nozzle. A modern approach (Radiatively Heated Wind Tunnel) uses an HF laser to excite the (02 1 1) mode of CO 2 naturally present or added to the flow. One of the early challenges in the development will be to demonstrate the ability to add energy into the supersonic flow in a predictable and controllable manner. Consequently, a subscale experiment, the Laser Demon-stration Device (LDD), is planned to investigate the transfer of laser energy to a small, expanding nozzle flow. Previous modeling of the energy transfer of the laser energy into the gas for the LDD depended on a conventional two-temperature approach to describe the internal structure of the molecules and to determine the rate coefficients. Realizing that the detailed physics of the energy transfer was important to the description of the wind tunnel performance and, hence, its viability, an effort was undertaken to compute the effect of CO 2 relaxation using a technique in which the individual vibrational states are considered. Results of these computations are reported here.

14. SUBJECT TERMS	15. NUMBER OF PAGES
vibrational relaxation, CO2, laser-heated flow, hypersonic flow, nozzle flow	16
	16. PRICE CODE

17. SECURITY CLASSIFICATION OF REPORT	18. SECURITY CLASSIFICATION OF THIS PAGE	19. SECURITY CLASSIFICATION OF ABSTRACT	20. LIMITATION OF ABSTRACT
Unclassified	Unclassified	Unclassified	UL